Article

Metal-Loaded Mesoporous MCM-41 for the Catalytic Wet Peroxide Oxidation (CWPO) of Acetaminophen

Mohammed Hachemaoui [1], Carmen B. Molina [2,*], Carolina Belver [2], Jorge Bedia [2], Adel Mokhtar [1,3], Rachida Hamacha [1] and Bouhadjar Boukoussa [1,4,*]

1   Laboratoire de Chimie des Matériaux L.C.M, Université Oran1 Ahmed Ben Bella, BP 1524, El-Mnaouer, Oran 31000, Algeria; mohamedb.f@live.fr (M.H.); mokhtar.adel80@yahoo.com (A.M.); rachidahamacha@gmail.com (R.H.)
2   Departamento de Ingeniería Química, Facultad de Ciencias, Campus Cantoblanco, UniversidadAutónoma de Madrid, E-28049 Madrid, Spain; carolina.belver@uam.es (C.B.); jorge.bedia@uam.es (J.B.)
3   Département Génie des Procédés, Institut des Sciences et Technologies, Centre Universitaire Ahmed Zabana Relizane, Relizane 48000, Algeria
4   Département de Génie des Matériaux, Faculté de Chimie, Université des Sciences et de la Technologie Mohamed Boudiaf, BP 1505, El-Mnaouer, Oran 31000, Algeria
*   Correspondence: carmenbelen.molina@uam.es (C.B.M.); bouhadjar.boukoussa@univ-usto.dz (B.B.); Tel.: +34-91-4972878 (C.B.M.); +213-771663458 (B.B.)

Abstract: MCM-41 based catalysts (molar ratio Si/Al = 40) were prepared by a hydrothermal route, modified by ionic exchange with different metals (Cu, Cr, Fe and Zn) and finally calcined at 550 °C. The catalysts were fully characterized by different techniques that confirmed the formation of oxides of the different metals on the surfaces of all materials. Low-angle X-ray diffraction (XRD) analyses showed that calcination resulted in the incorporation of metallic Zn, Fe and Cr in the framework of MCM-41, while in the case of Cu, thin layers of CuO were formed on the surface of MCM-41. The solids obtained were tested in the catalytic wet peroxide oxidation (CWPO) of acetaminophen at different temperatures (25–55 °C). The activity followed the order: $Cr/MCM\text{-}41 \geq Fe/MCM\text{-}41 > Cu/MCM\text{-}41 > Zn/MCM\text{-}41$. The increase of the reaction temperature improved the performance and activity of Cr/MCM-41 and Fe/MCM-41 catalysts, which achieved complete conversion of acetaminophen in short reaction times (15 min in the case of Cr/MCM-41). Fe/MCM-41 and Cr/MCM-41 were submitted to long-term experiments, being the Fe/MCM-41 catalyst the most stable with a very low metal leaching. The leaching results were better than those previously reported in the literature, confirming the high stability of Fe/MCM-41 catalysts synthesized in this study.

Keywords: mesoporous materials; Al-MCM-41; metal loaded; CWPO; acetaminophen; stability

1. Introduction

In recent years, global concern about the presence of pharmaceutical compounds in water has significantly increased. A wide variety of pharmaceutical compounds, such as analgesics, anti-inflammatory, antibiotics, contrast or antiepileptic agents, has recently been detected in many water resources [1]. The pharmaceutical compounds found in the environment come mainly from the elimination of these molecules and their metabolites by humans or animals under therapeutic treatment and/or and inadequate treatment of manufacturing effluents [2]. Because of their stabilities and sometimes recalcitrant behavior, they are not completely removed/degraded by conventional wastewater treatment techniques [3–5]. Their concentrations in water, although depending on the specific site and compound, are generally low, in the range of micrograms to nanograms per liter [3–5], although in the case of wastewaters coming from manufacturing plant effluents they could

be found at higher concentrations. Acetaminophen (ACE) is one of the most used pharmaceutical compounds at global scale. It has very few adverse effects especially at the gastrointestinal level compared to other analgesics and/or antipyretics. The occurrence of pharmaceuticals in water bodies has raised a concern due to their negative effects on both environment and human health. Pharmaceutical pollutants can result in increasing aquatic toxicity, the development of resistance in pathogenic bacteria, endocrine disruption and/or genotoxicity [6,7]. Therefore, the development of effective treatments to remove this contaminant in aquatic environments is an important environmental goal. Adsorption and advanced oxidation processes (AOPs), including photocatalysis and catalytic wet peroxide oxidation (CWPO), are among the most used methods for the removal of acetaminophen from water [8–12].

AOPs have proven to be capable and effective to completely degrade pharmaceutical compounds from aqueous solutions. For this purpose, different catalysts have been tested, such as metal oxides [13–16], oxide metal containing mesoporous silica Santa Barbara Amorphous-15 (SBA-15) [17], metal nanoparticles (NPs) supported on organic-inorganic matrix [18], metal containing zeolite [19], metal–carbon xerogels [20] or clays [21,22], among many others. In all cases, the catalysts used for this type of reactions require the presence of active transition metals in the form of oxides, nanoparticles or zero-charge metallic species. The choice of the nature of the metal and the support plays a very important role on the catalytic activity, selectivity and stability of the reaction. A priori, the use of well-dispersed transition metals on supports with high specific surface area and high thermal and hydrothermal stabilities can be considered a good option to achieve the reaction requirements. In this sense, mesoporous silicas have focused much interest [23–25]. These solids have high surface areas and well-developed mesoporous structure with adjustable and high pore size compared to zeolites [26–28]. They can be used without calcination as basic catalysts in several reactions due to the presence of siloxy ($\equiv SiO^-$) as basic sites [29,30]. Their catalytic oxidation/reduction properties differ according to the nature and the form of the supported metal, as well as the method used for the dispersion of the metal on the surface of the mesoporous silica [31–33]. The most widely used methods are post-synthesis methods or direct methods [30–33]. Post-synthesis methods provide a great potential for loading metal into the pore channels, and excellent mesoporous structure compared to the direct method, which has a limited percentage of metal to avoid the collapse of the structure of the mesoporous silica [31]. Usually, the synthesis of mesoporous silica finishes with a calcination step devoted to the removal of the organic template and the condensation of the silanol groups. To date, the calcined form of mesoporous silica is widely used for the dispersion of metals or metal oxide on their surfaces [31–33]. In contrast, the non-calcined form has been scarcely described in the literature. In this study, we have selected a non-calcined mesoporous Mobil Composition of Matter-41(MCM-41) due to its hexagonal 2D structure and adjustable pore diameter, with the aim of increasing the amount of metal loaded in the subsequent ionic exchange. The catalysts were subsequently submitted to calcination, after metal loading. According to our knowledge this approach has never been studied in the oxidation of acetaminophen.

Among the different AOPs, the CWPO process has been widely analyzed [13,34]. This technology is characterized by low investment and operating costs and a relatively high efficiency. CWPO, also known as heterogeneous Fenton, reduces the generation of Fe hydroxide sludges when compared to conventional homogeneous Fenton processes. However, CWPO suffers from stability problems produced by deactivation of the catalysts due to the surface complexation of metal ions (usually iron ions) with short-chain acids and lixiviation [35]. This problem can result in an incomplete mineralization (degradation to CO_2 and H_2O_2) of the organic matter present in the water. Moreover, the high consumption of H_2O_2, which constitutes the main cost of the process, limits the practical application of this technology. The search of active and stable CWPO catalysts is crucial for the implement of this technology.

The main objective of this work is the preparation of different mesoporous materials containing different transition metals (Cu, Cr, Fe and Zn) using the non-calcined form of MCM-41 in order to increase the metal loading of the final catalysts. The catalysts were tested in the CWPO of acetaminophen and the proper structure-performance relationships were detailed and discussed.

2. Results

2.1. Characterization of the Catalyst

Figure 1 represents the X-ray diffraction (XRD) patterns at low and large angles of MCM-41 and the different catalysts. The XRD pattern of the original MCM-41 sample shows the presence of an intense peak at a 2θ value close to 2.5°, besides to lower intensity peaks at 2θ values around to 3.7 and 4.3°, characteristic of the reflection of (100), (110) and (200) planes of this mesoporous solid aluminosilicate. The absence of peaks at higher angles is because MCM-41 consists of amorphous silica, and thus it has no crystallinity at the atomic level [36] but only a high pore ordering. The different catalysts show clear differences in the XRD patterns. Cu/MCM-41 catalyst retains a high intensity (100) peak, besides two lower intensity peaks (110) and (200) at $2\theta \approx 3.72$ and 4.30°, respectively. This confirms that this sample maintains the hexagonal structures of the MCM-41 with a high degree of structural ordering [37]. The XRD patterns of the rest of the catalysts, Cr/MCM-41, Fe/MCM-41 and Zn/MCM-41, show much lower intensity of (100) peak and are displaced to lower diffraction angles. This can be explained by the swelling of the hexagonal mesh due to the incorporation of the metal in the MCM-41 framework (see Table 1) in agreement with previous observations [30,38]. The modification of the mesh parameters confirms that the calcination at 550 °C leads to the incorporation of the metal in the inner of the MCM-41 framework. The incorporation of a metal into the framework of the MCM-41 causes an increase in the mesh parameter depending on the size of the radius of the metal introduced in its structure [30,39]. According to the calculated values of a_0, it is shown that all the modified materials have higher values compared to the parent MCM-41, except Cu/MCM-41 catalyst, which has an almost similar value compared to the parent MCM-41. In the large angles, all the catalysts presented new phases corresponding to the oxides of the metals added in the ion exchange process on the surface of MCM-41. Hence, the peaks at 2θ values of 35.5, 38.7, 42.3, 48,7 and 52.4° correspond to the (−111), (111), (200), (−202) and (211) reflection phases of CuO respectively [38,40]. In the case of Fe/MCM-41 catalyst, new peaks show up at 2θ values around 33.1, 35.6, 40.0, 43.0, 50.0 and 53.1° characteristic of the (104), (110), (113), (202), (024) and (116) reflection phases of Fe_2O_3, respectively [41,42]. Finally, Cr/MCM-41 catalyst shows diffraction peaks at 2θ close to 33.6, 36.2, 41.4, 50.2 and 54.8° characteristic of the (104), (110), (113), (023) and (116) diffraction planes of Cr_2O_3, respectively [43,44]. This confirms that the calcination does not only lead to the incorporation of the metal into the MCM-41 framework but also forms metal oxides phases on its surface. Cu/MCM-41 catalyst has the higher intensity peaks in the region 30–60° probably due to the formation of higher crystalline CuO outside the MCM-41 framework. This result, besides the low significant modification of the a_o parameter, suggests than in the case of Cu, most of the metal was not incorporated into the Al-MCM-41 framework but deposited on the surface in CuO form. In the case of the Zn exchange, no ZnO phase was observed for the Zn/MCM-41 sample, suggesting this metal was deposited in the form of well-dispersed species with small size [36].
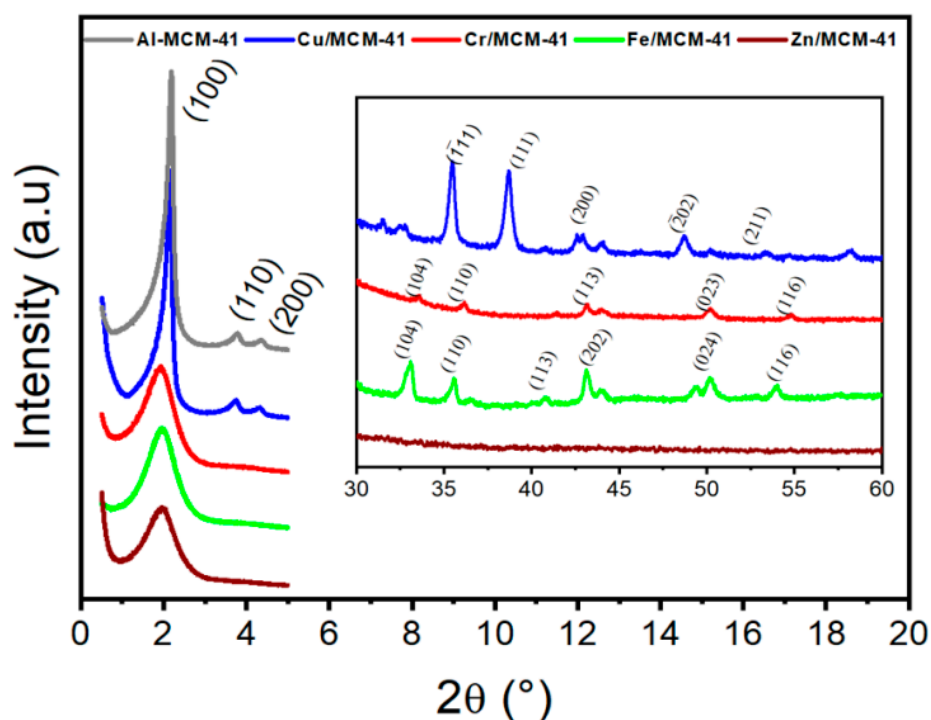
Figure 1. X-ray diffraction (XRD) patterns of calcined Al-MCM-41 and its modified counterparts.

Table 1. Structural and textural properties of MCM-41 and its modified counterparts.

	Metal [a] (%)	d_{100} (nm)	a_0 [b] (nm)	S_{BET} (m²/g)	Pore Volume (cm³/g)	Pore Size [c] (nm)
MCM-41	//	4.085	4.716	1100	1.031	3.670
Zn/MCM-41	0.97	4.524	5.224	650	0.643	4.038
Fe/MCM-41	4.36	4.570	5.277	640	0.738	4.416
Cu/MCM-41	0.94	4.109	4.745	950	0.727	3.570
Cr/MCM-41	1.91	4.555	5.259	780	0.694	3.856

[a] Metal content determined by X-ray fluorescence (XRF) analysis. [b] a_0 means lattice parameter: $a_0 = 2d_{100}/\sqrt{3}$. [c] Pore diameter determined by the BJH method.

The ion metal exchanged with Cetyltrimethylammonium(CTA$^+$) in MCM-41 before calcination increases the incorporation inside the material [45–47] which means more metal oxide, the amount of the metal in each catalyst was quantified by X-ray fluorescence (XRF) being summarized in Table 1. Fe/MCM-41 and Cr/MCM-41 showed the highest percentage of metal compared to those of Cu/MCM-41 and Zn/MCM-41.

The nitrogen adsorption-desorption isotherms at 77 K of the different catalysts and the pattern MCM-41 are represented in Figure S1. All isotherms are of type IV characteristic of mesoporous materials with also a significant presence of microporosity [29,30,48]. These isotherms are characterized by three steps; the first step is carried out at low relative pressures (P/P$_0$ < 0.25) which are characteristic of monolayer adsorption of nitrogen on the micropore walls. The second step takes place at relative pressures between 0.25 < P/P$_0$ < 0.4 which is characterized by a sharp increase in nitrogen adsorption. This adsorption behavior is due to capillary condensation within the uniform micropores. The third step starts from P/P$_0$ > 0.4 which corresponds to the gradual increase in volume, due to the multilayer adsorption on the outer surface of the mesoporous materials. Table 1 shows the textural properties of obtained materials. It can be seen that the exchange of MCM-41 with the different metals resulted in a reduction of the porosity of the resulting catalysts [29,30]. This is strongly related to the particle blocking of the internal porosity by the incorporation of the metallic species. The increase of the pore diameter compared to the parent material

is due to the incorporation of the incorporation of the metals to the structure during the heat treatment. Fe/MCM-41 exhibited the highest pore diameter suggesting a significant incorporation of this metal into the framework of the MCM-41, while Cr/MCM-41 exhibited a slight modification (in agreement with the amount of metal quantified by XRF). The catalyst Cu/MCM-41 has the higher surface area compared to the other modified samples probably due to its low metal content (see Table 1). This result confirms that CuO was deposited in the wider mesopores of MCM-41, which is in agreement with previously published works [48].

The study of the thermal behavior of the materials obtained makes it possible to determine the mass loss of each sample with increasing temperature, but also provides information about the formation mechanism of metal-loaded-MCM-41. Figure S2 shows the thermogravimetric analysis (TGA) curves under nitrogen atmosphere (inert atmosphere to avoid weight gaining caused by the presence of oxygen in air atmosphere) of as-synthesized MCM-41 (parent material) and its counterparts modified by Cr, Fe, Zn and Cu, prior to calcination. All materials presented two masses losses, the first mass loss occurs between 25 and 120 °C and it is associated to the loss of physiosorbed water. The second mass loss takes place at temperatures between 120 and 700 °C and corresponds to different stages of degradation of the surfactant CTA^+.

Infrared spectroscopy was used in order to determine qualitatively the different groups of the catalysts before and after calcination (Figure S3). After calcination at 550 °C a wide band was formed at 3387 cm^{-1} and another band appears at 1635 cm^{-1} (Figure S3b). These bands are due to the presence of the silanol groups and also to the vibrations of physiosorbed water. This also confirms that calcination not only removes the surfactant inside the pores of MCM-41, as indicates the disappearance of the bands at 2919 and 2848 cm^{-1}, but also leads to the formation of higher amounts of silanol groups compared to non-calcined materials. The bands at 1221, 1032 and 786 cm^{-1} for the non-calcined materials have been moved to 1238, 1048 and 794 cm^{-1} at the higher wavenumbers, respectively. This behavior is strongly linked to the incorporation of transition metals into the framework of MCM-41 due to the calcination treatment [49].

Ultraviolet–visible (UV–vis) spectroscopy was used in order to determine the coordination nature of the metallic species supported on the surface of MCM-41. As shown in Figure S4, the bare mesoporous silica only shows peaks at wavelengths in the 200–350 nm range corresponding to UV absorption of SiO_2 [50]. The introduction of Cu, Zn, Fe and Cr in MCM-41 results in significant changes in the corresponding UV–Vis spectra (Figure 2). The catalyst Cu/MCM-41 displays two clear bands, an intense band at 219 nm and a wide band between 300–800 nm that are mainly due to the presence of Cu^{2+} in form of CuO NPs [51,52]. Zn/MCM-41 catalyst is characterized by two bands, the first is located at 257 nm and the second and wide band located at 305 nm, which can be assigned to encapsulated ZnO NPs [53,54]. In general, the band below 220 nm confirms the incorporation of Zn into the framework of MCM-41 and is associated with the charge transfer transitions of the zinc species with the oxygen of the framework [55]. The UV spectrum of the catalyst Cr/MCM-41 is very similar to that obtained in the literature in which it clearly shows the existence of Cr_2O_3 [56]. The catalyst Fe/MCM-41 presents a strong band at 215 nm associated with another band at 268 nm, which is assigned to the charge transfer between the Fe^{3+} and O^{2-} atoms (Fe–O–Si) in the framework of MCM-41 [57]. In addition to these bands, a shoulder appeared around 330 and 500 nm, indicating the presence of either extra-framework iron or iron oxide particles [58].
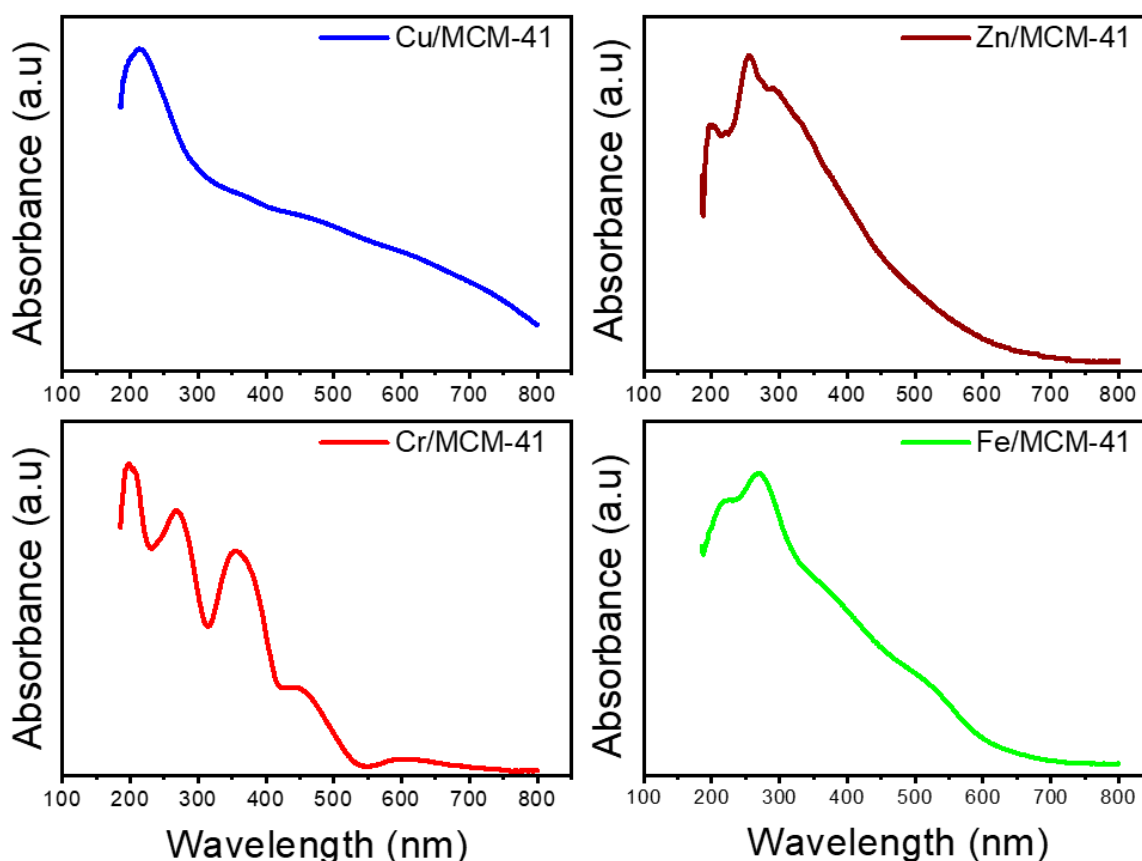
Figure 2. Ultraviolet–visible (UV–vis) spectra of the calcined M/MCM-41 catalysts.

The investigation of the electronic states of MCM-41 doped by different metals was carried out by X-ray photoelectron spectroscopy (XPS). Figure 3 represents the Cr, Cu, Zn and Fe 2p XPS signal of the correspondent catalysts. XPS spectra of Cr 2p showed the Cr $2p_{1/2}$ and Cr $2p_{3/2}$ peaks on Cr/MCM-41 were located at 586.3 and 576.7 eV, which are characteristic of Cr_2O_3 species [59,60]. The O1s XPS peak (Figure S5 of the Supplementary DATA) has a peak at 532 eV, which corresponds to the oxygen of the Cr_2O_3 network [53] and also to the Si-O bond and explains a close interaction between oxygen and silicon [61]. The XPS spectra of Cu 2p of the catalyst Cu/MCM-41 have two Cu peaks, belonging respectively to Cu $2p_{3/2}$ at around 933 eV and Cu $2p_{1/2}$ at 953 eV, suggesting the presence of Cu^{2+} species in form of CuO [62,63]. The Zn 2p peaks for the catalyst Zn/MCM-41 show the Zn $2p_{1/2}$ and Zn $2p_{3/2}$, contributions, with peaks at 1045.8 eV and 1022.6 eV ascribed to Zn^{2+} species [64]. The value of Zn $2p_{1/2}$ –Zn $2p_{3/2}$ is approximately 23.12 eV corresponding to the typical splitting value of ZnO [65,66]. The Fe 2p XPS spectra of Fe/MCM-41 exhibited a strong peak at 711.0 eV with a lower intensity satellite peak at 719.2 eV assigned to Fe $2p_{3/2}$ signal. The weak satellite peak of around 719.52 eV is characteristic of Fe^{3+} in Fe_2O_3 [67]. The binding energy of Fe $2p_{1/2}$ is around 724.84 eV associated with other satellite peak at 732.01 eV [68]. The peaks at around 711.01 eV and 724.84 eV, indicating Fe components were mainly in trivalent status in Fe-MCM-41 [69]. The XPS O1s peak of all the catalysts is very similar (see Figure S5). A first peak, between 533.0–533.2 eV, corresponds to the oxygen of SiO_2 [70]. The other peak, located at around 532.0–530.0 eV, is attributed to T–OH (T = Si, Al or Metal), T–O–Si (T = Metal) and T–O (T = Metal) [70–72]. These peaks were almost masked by the intense and wide oxygen signal from SiO_2 [73].
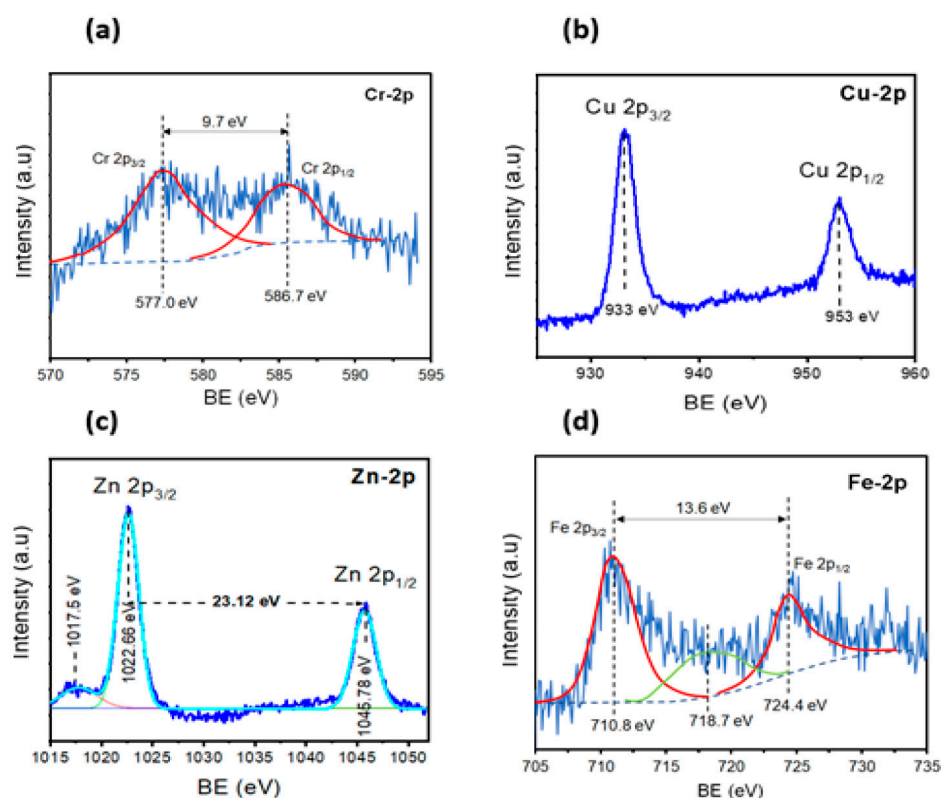
Figure 3. Cr (**a**), Cu (**b**), Zn (**c**) and Fe (**d**) 2p X-ray photoelectron spectroscopy (XPS) signal of the corresponding calcined catalysts.

2.2. Catalytic Test

Figure 4a,b represent the ACE concentration and H_2O_2 conversion upon reaction time when using the different catalysts. It should be remarked that the ACE adsorption (see Figure S6) was negligible in all th siloxy e cases. Despite the well-developed surface area of the MCM-41 sample, it shows an almost negligible adsorption capacity of acetaminophen. This is mainly due to the hydrophilic nature of MCM-41, and it is in agreement with previous studies [74]. All the tests were performed at pH = 3, which is generally accepted as the optimal pH to perform CWPO reactions. At lower pH values the formation of hydrated metal complexes results in a lower production of hydroxyl radicals. Furthermore, at very acidic conditions a higher number of protons is free in the medium to react with hydroxyl radicals, which decreases the overall efficiency of the process. On the other hand, pH > 4 favors the formation of metal oxyhydroxides on the catalyst's surface, which inhibits both the production of hydroxyl radicals and the regeneration of the metal ions. ACE conversion varies in the following sequence Cr/MCM-41 >> Fe/MCM-41 > Cu/MCM-41 >> Zn/MCM-41. The ACE conversion was completed in less than 60 min using Cr/MCM-41 while the Fe/MCM-41 catalyst needs four times higher reaction time to achieve complete ACE conversion. The low initial acetaminophen concentration (5 mg·L^{-1}) makes difficult the identification and accurate quantification of the reaction intermediates. No additional aromatic compounds were observed in HPLC chromatograms. However, short-chain organic acids, such as, oxalic, acetic and formic acids, were detected using ionic chromatography. The difference between the ACE and H_2O_2 final conversions (at 4 h) when using Fe/MCM-41 catalyst should be ascribed to the presence of intermediate oxidation byproducts, suggesting an incomplete mineralization of ACE. In contrast, Zn/MCM-41 catalysts showed very little ACE conversion, hardly 10% after 240 min of reaction. This activity can be linked to several factors such as the nature of the metal oxides, their crystallinity, their metal particle sizes and/or their specific surface [75,76]. The results illustrated in Figure 4 are not in agreement

with the trend observed for the microporosity of the samples, suggesting that the catalytic activity of the catalysts is not strongly affected by the surface, as previously reported in other studies [20].
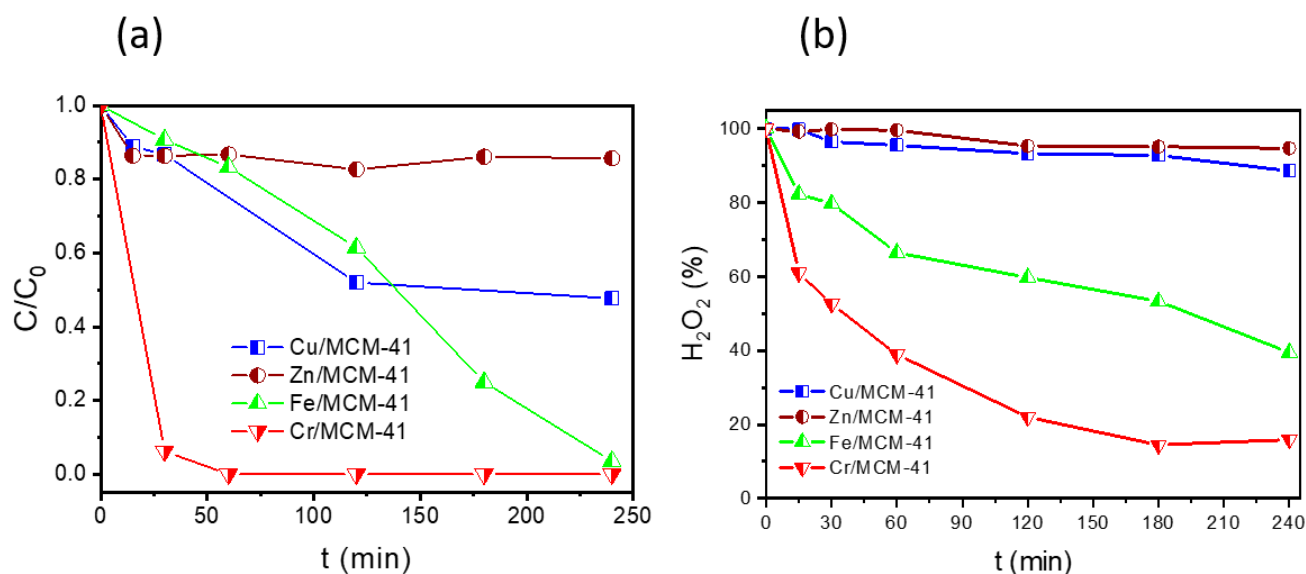

Figure 4. Effect of the metal introduced in the catalyst: (**a**) Time-course of acetaminophen (ACE) evolution and (**b**) H_2O_2 conversion with the synthesized catalysts (ACE initial concentration: 5 mg/L; catalyst concentration: 1 g/L, reaction temperature: 25 °C, H_2O_2: stoichiometric amount, pH_i: 3).

The low activity of Cu/MCM-41 and Zn/MCM-41 catalysts was probably linked to their lower metal content (Table 1). Moreover, these samples have not been able to decompose H_2O_2, which justifies their lower activity in CWPO reaction. Fe/MCM-41 and Cr/MCM-41 catalysts have higher metal contents. Several studies have shown that the various oxide metals including magnetite [34,77,78] are effective heterogeneous Fenton catalysts which are in agreement with our results.

The best catalysts, Fe/MCM-41 and Cr/MCM-41, were used in the rest of the work. Figure 5 represents the evolution of ACE concentration and H_2O_2 conversion with reaction time when using different loads of Fe/MCM-41 and Cr/MCM-41 catalysts. The mass of catalyst was varied between 0.5 and 2 g/L while keeping the temperature (25 °C) and pH ≈ 3 of solution constant. The load of catalyst plays a very important role on the conversion of ACE that increases rapidly with increasing mass of the catalyst. A total conversion of ACE was obtained with Cr/MCM-41 catalyst at reaction time lower than 30 min when using catalyst loads of 1 or 2 g/L. This is a consequence of the presence of more active sites when using higher loads of catalyst. Another explanation also linked to the size of the chromium oxides which probably have a smaller size compared to the iron oxides, Cr/MCM-41 has a larger surface area than Fe/MCM-41, which may be due to the presence of large particles of iron oxide inside the pores subsequently leading to a decrease in the number of sites, and thus a tortuous diffusion of reagents.

Figure 5c,d shows H_2O_2 conversion using both catalysts. In the case of Cr/MCM-41, higher conversions of H_2O_2 lead to higher and faster degradation of ACE. It should be noted that the reaction between H_2O_2 and ACE without catalyst does not lead to any degradation which has been confirmed by Carrasco-Díaz et al. [20]. It has been shown that the total degradation of ACE requires approximately 45–55% of H_2O_2 conversion for the case of Cr/MCM-41 catalyst. While for the Fe/MCM-41 catalyst, approximately 20–30% of H_2O_2 conversion was recorded to have a total degradation of ACE. It has already been shown in the literature that the use of a solution pH in the range 2.8–3.2 generates at the same time the coexistence of three active species Fe^{2+}, Fe^{3+} and $[Fe(OH)]^{2+}$ [79], which are considered as Fenton-active sites for the degradation of ACE. The H_2O_2 decomposition

mechanism has already been described in the literature confirming the intervention of these three species in the degradation of pollutants [78,79].
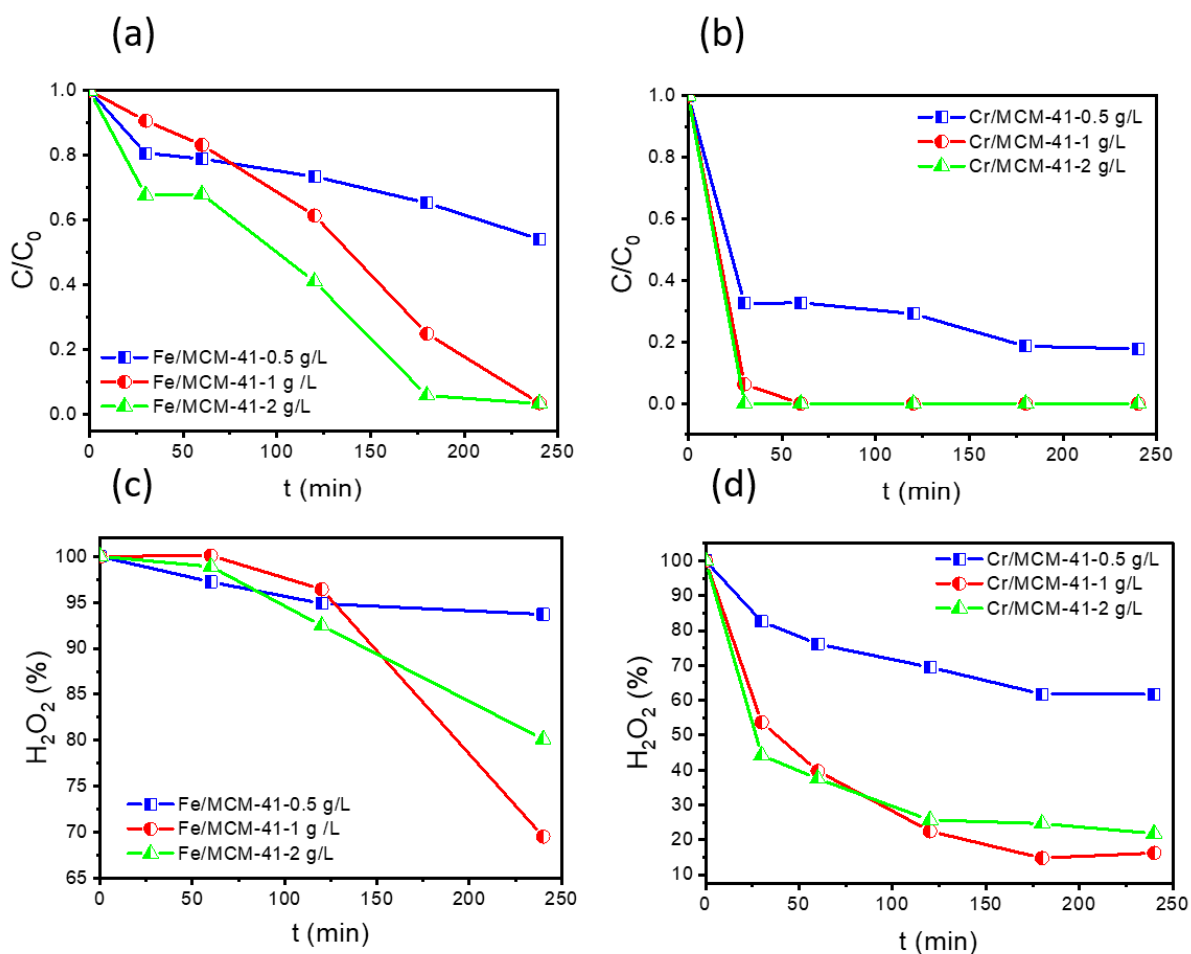

Figure 5. Effect of catalyst concentration: time-course of acetaminophen evolution using as catalysts Fe/MCM-41 (**a**) and Cr/MCM-41 (**b**); H_2O_2 conversion using as catalysts Fe/MCM-41 (**c**) and Cr/MCM-41 (**d**) (ACE initial concentration: 5 mg/L; reaction temperature: 25 °C, H_2O_2: stoichiometric amount, pH_i: 3).

Figure 6 summarizes the effect of reaction temperature (25–55 °C) using Fe/MCM-41 and Cr/MCM-41 catalysts. Higher reaction temperatures favor the reaction rate of ACE and the H_2O_2 decomposition. The decomposition of H_2O_2 increases significantly when the temperature increases from 25 to 55 °C, which can be explained by a higher conversion of ACE, as previously reported with other pollutants as phenol [80]. Concerning the Cr/MCM-41 catalyst, only a slight increase in the ACE removal was observed (Figure 6b) although the conversion of H_2O_2 was higher at higher reaction temperature (Figure 6d) due to its higher catalytic activity, with room temperature enough to achieve a total degradation of ACE. However, Fe/MCM-41 exhibited a lower catalytic activity and a higher temperature of 55 °C was necessary to reach similar results than those obtained with Cr/MCM-41. When using Fe/MCM-41 catalysts the reaction rate increases with the reaction temperature. Using the Arrhenius equation (Equation (1)) the activation energy for the acetaminophen degradation is 86 kJ·mol^{-1} (see Figure S7). In the case of Cr/MCM-41 the degradation is very fast at the reaction temperatures analyzed and no accurate value of the activation energy can be obtained. The Turnover Frequency (TOF) (Equation (2)) has been calculated as the mols of acetaminophen converted per mol of metal in the catalysts and per unit of time. At 25 °C, Fe/MCM-41 and Cr/MCM-41 catalysts show TOF values

for the acetaminophen degradation of c.a. $1.7 \cdot 10^{-4}$ and $5.4 \cdot 10^{-3}$ min^{-1}, respectively, which confirms the higher activity of Cr than Fe.

$$\frac{dlnK}{dT} = \frac{Ea}{RT^2} \tag{1}$$

$$TOF_{ACE} = \frac{\text{Acetaminophen converted (mol)}}{\text{Metal in solid (mol)} \cdot \text{Reaction time (min)}} \tag{2}$$
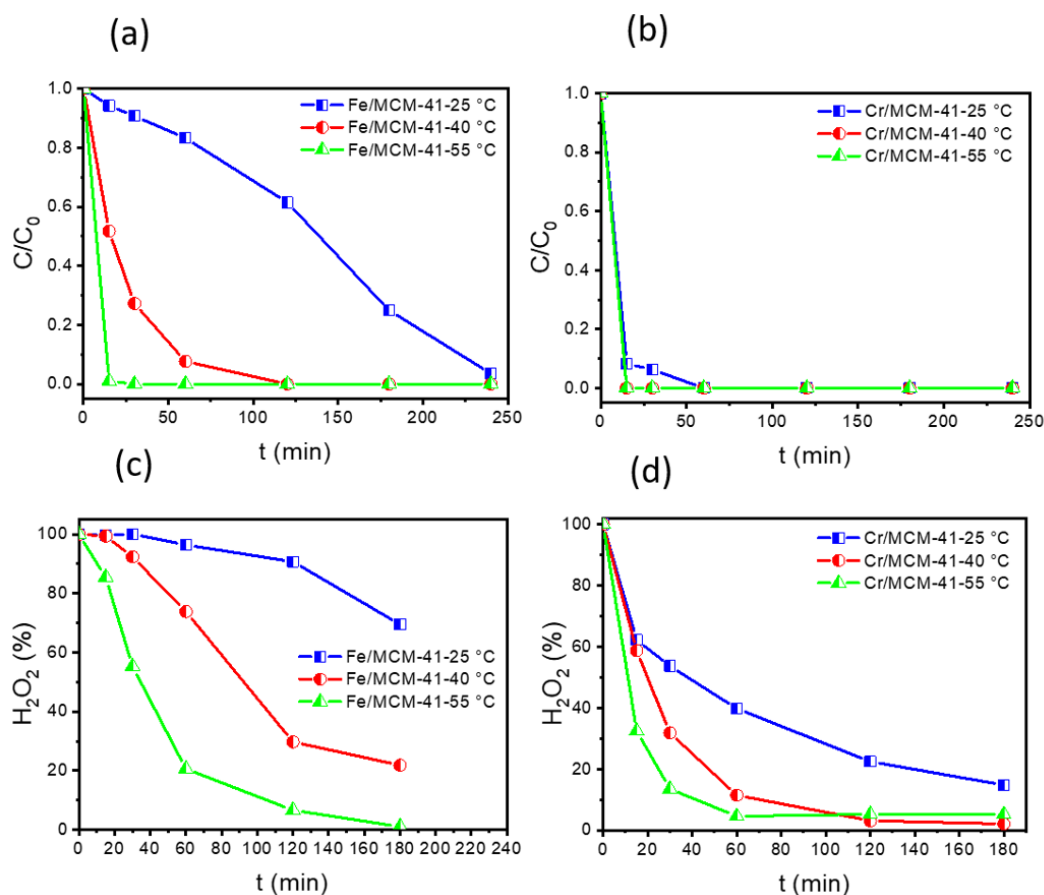

Figure 6. Effect of reaction temperature: time-course of acetaminophen evolution using as catalysts Fe/MCM-41 (**a**) and Cr/MCM-41 (**b**); H_2O_2 conversion using as catalysts Fe/MCM-41 (**c**) and Cr/MCM-41 (**d**) (ACE initial concentration: 5 mg/L; catalyst concentration: 1 g/L; H_2O_2: stoichiometric amount, pH_i: 3).

The stability of the catalysts was tested in continuous tests for seven days. shows the evolution of ACE concentration and H_2O_2 conversion in those long-run tests. The two catalysts are very stable under the reaction conditions for seven consecutive days. The catalytic activity of each material was stable without losing their performance. The conversion of H_2O_2 was constant during the seven days of treatment, which results in a total degradation of ACE. To completely assess that the catalyst does not suffer significant modification after long reaction times, additional characterization of the used catalyst is necessary. However, the results shown here allow us to state that the catalyst is capable to maintain the high acetaminophen conversion at those extremely long reaction times. Metal leaching has been studied in order to confirm the possible contribution of homogeneous Fenton to the degradation of ACE. These results confirm the stability of the Cr/MCM-41 and Fe/MCM-41 catalysts prepared by a simple process which consists in a partial exchange between metal and CTA$^+$ followed by calcination.
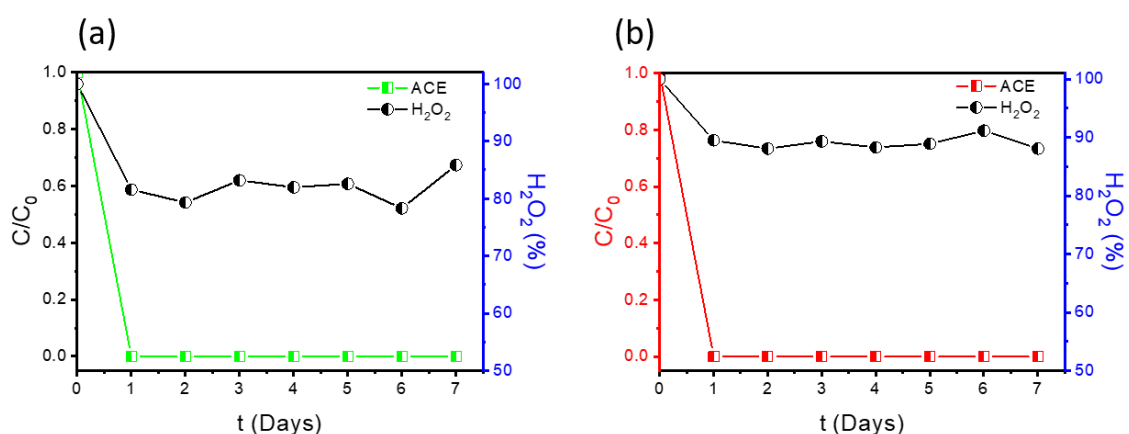
Figure 7. Long-term experiments with Fe/MCM-41 (**a**) and Cr/MCM-41 (**b**) catalysts (ACE initial concentration: 5 mg/L; catalyst load: 0.1 g; ACE solution flow: 0.243 mL/min; H_2O_2: stoichiometric amount, pH_i: 3).

The mechanism of the oxidation of acetaminophen has been extensively studied in the literature (Figure 8). In the case of CWPO of acetaminophen, the reaction pathway begins with the formation of benzoquinone, which result upon further oxidation in the generation of benzaldehyde and benzoic acid [81–83]. These by-products further decompose in smaller aliphatic organic acids such as maleic, oxalic, acetic and formic acids, which are non-toxic products [82,83]. The last step involves the complete mineralization to CO_2, H_2O and NO_3^-.
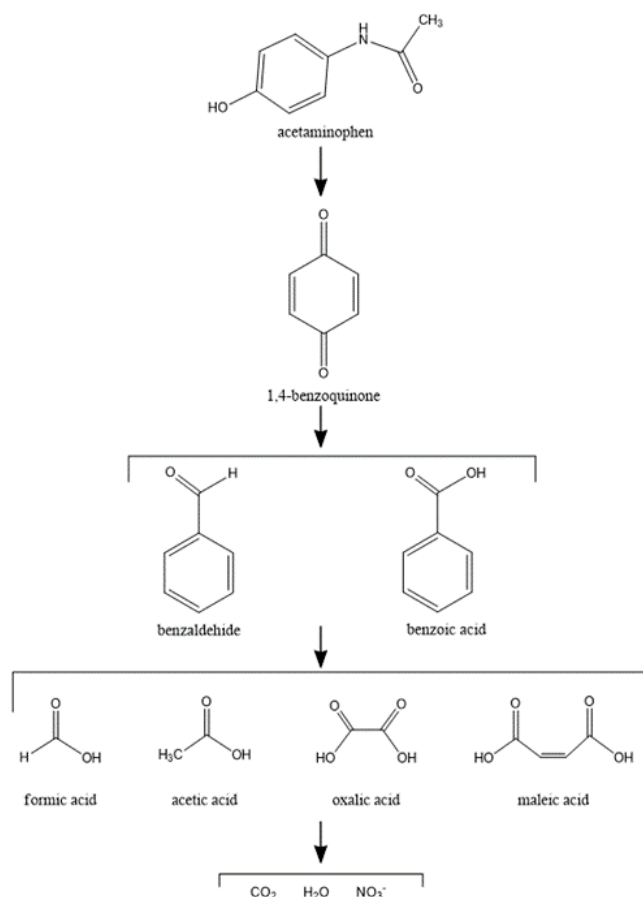

Figure 8. Tentative acetaminophen degradation pathway.

3. Materials and Methods

3.1. Materials

Cetyltrimethylammonium bromide (CTABr, 98%, Alfa Aesar), tetraethyl orthosilicilate (TEOS, 98%, Sigma-Aldrich), aluminium isopropoxide (98%, Acros Organics), NaOH (98%, Biochem Chemopharma), $CuNO_3 \cdot 4H_2O$ (95%, Biochem Chemopharma), $CrNO_3 \cdot 9H_2O$, (99%, Sigma Aldrich), $FeCl_3 \cdot 6H_2O$ (97%, Sigma Aldrich) and $ZnNO_3 \cdot 6H_2O$ (98%, Sigma Aldrich) were employed in the study. All reagents were used without further purification. The aqueous solutions were prepared with deionized water.

3.2. Catalyst Preparation

Mesoporous MCM-41 support was synthesized by a hydrothermal method as reported elsewhere [29,30,84]. The molar composition used in the formulation was Si/Al = 40, 0.12 CTAB, 0.25 NaOH, 1.5 EtOH and 100 H_2O. Briefly, an aqueous solution with CTABr surfactant and ethanol was prepared at a temperature of 35 °C. After homogenization of the mixture, TEOS was added dropwise at the same time with a solution containing distilled water, sodium aluminate and NaOH in the solution containing the surfactant. The reaction mixture was placed under constant stirring for 3 h at 35 °C, after the product was hydrothermally treated at 100 °C for two days. The final product was filtered, washed several times with distilled water and then dried at 60 °C. Different transition metals (Cu, Cr, Fe and Zn) were exchanged on the MCM surface in order to obtain the CWPO catalysts. About 2 g of as-synthesized MCM-41 was dispersed in 100 mL of 0.1 M solutions of the different metal salts and stirred for 2 h at room temperature. Then the mixture was filtered, washed several times with distilled water and dried overnight at 60 °C. For the release of the porosity of the obtained materials through the removal of the organic template and the condensation of the silanol groups, the product was calcined for 6 h at 550 °C in an air atmosphere (to improve the formation of metal oxides in air oxygen). The catalysts were named as M/MCM-41 being M the metal exchanged (Cr, Fe, Cu and Zn) [49,85].

3.3. Catalysts Characterization

XRD powder diffraction patterns of calcined samples were obtained with a Bruker AXS D-8 diffractometer using Cu-Kα radiation at 2θ = 1–60°. Nitrogen adsorption-desorption isotherms were obtained at −196 °C using ASAP 2020 Micromeritics apparatus. The samples were previously outgassed at 100 °C for 10 h prior to the sorption measurements. The thermal properties and mass losses were followed by means of a thermobalance (TGA DISCOVERY SDT-650) under nitrogen flow. The functional groups of the metal-modified MCM-41 before and after calcination were analyzed by Fourier transform infrared (FTIR) spectra in the range of 500–4000 cm^{-1} using a BRUKER ALPHA Platinum-ATR instrument. The metal coordination state with the mesoporous silica was analyzed by ultraviolet visible (UV–vis) absorbance spectra using SHIMADZU UV-2700 spectrometer. The amount of metal in each sample was determined by X-ray fluorescence using a XEPOS spectrometer (Spectro Ametek). The XPS measurements were carried out on a Kratos Axis Ultra using AlKα (1486.6 eV) radiation. High-resolution spectra were acquired at 20 eV pass energy with energy resolution of 0.9 eV, the C1s line of 284.5 eV was used as a reference to correct the binding energies for charge energy shift.

3.4. Adsorption Tests

The adsorption tests were performed in batch reactor at 25, 40 and 55 °C. Briefly, 1 g of catalyst was added to a 5 mg/L of ACE solution (1000 mL) at a fixed pH close to 3 using a 1 M HCl solution. The samples were taken at different times in maximum 2 h and they were analyzed by high-performance liquid chromatography (HPCL) in order to obtain the adsorption capacities of catalysts. The results show that adsorption equilibrium was obtained after 1 h with very low adsorption capacities.

3.5. Catalytic Tests

CWPO tests were carried out in batch reactor at controlled temperature. A catalyst concentration of 1 g/L was used while the ACE initial concentration was fixed at 5 mg/L. The pH was adjusted to 3 using a 1 M HCl solution. The mixture was stirred for 1 h in order to achieve adsorption equilibrium and then the stochiometric amount of H_2O_2 was added to the solution to initiate the reaction. The conversion of ACE was followed by HPLC (Shimadzu Prominence-I LC-2030C with a diode array detector) at a wavelength of 246 nm using a reverse phase C18 column. A mixture of acetonitrile/acetic acid 0.1% *v/v* was used as mobile phase (0.7 mL/min). The effects of the metal active phase, catalyst mass (0.5, 1.0 and 2.0 g/L), and reaction temperature (25, 40 and 55 °C) were analyzed.

The stability of catalysts was investigated using a continuous reaction test for one week. An ACE solution was continuously fed to the reactor (0.243 mL/min) using the best catalysts (100 mg) at a reaction temperature of 25 °C. The same volume of solution was extracted and analyzed to follow the ACE conversion with time on stream. The H_2O_2 concentration in the reaction medium was quantified by colorimetric methods with a Cary 60 UV–Vis (Agilent Technologies) spectrophotometer, using the titanium oxisulphate method [86].

4. Conclusions

The mesoporous material MCM-41 with a Si/Al ratio = 40 was prepared by a hydrothermal method. The as-synthesized MCM-41 was ionic exchanged with several transition metals such as Fe, Cr, Cu and Zn and then calcined at 550 °C. The results (XRD, XPS, UV–vis, FTIR) showed that Fe, Cr, Cu and Zn were incorporated into the MCM-41 framework, which was confirmed by the inflation of the mesh parameter (a_0 of the modified materials was higher compared to the parent material), and a part of the metals were transformed in their corresponding oxides form (Fe_2O_3, ZnO, CuO and Cr_2O_3). The nitrogen adsorption at 77K showed that the surface area was reduced due to the pores blockage by metal oxides. However, different behavior was observed for the catalyst Cu/MCM-41 in which the formation of CuO thin layers slightly decreased the surface area.

Application of these solids in the oxidation of ACE showed that the ACE conversion varies in the following sequence Cr/MCM-41 > Fe/MCM-41 > Cu/MCM-41 > Zn/MCM-41. The effect of the initial concentration of ACE, reaction temperature and the catalyst mass were studied in which the Cr/MCM-41 and Fe/MCM-41 catalysts were judged as the best catalysts for this kind of reaction. The use of both these catalysts in long-time tests showed that ACE conversion was higher and stable, which confirms the high stability of the synthesized catalysts.

Author Contributions: Conceptualization, M.H., C.B.M., C.B., J.B., A.M., R.H., B.B.; methodology, M.H., C.B.M., C.B., J.B.; writing—original draft preparation, M.H., C.B.M., J.B.; writing—review and editing, M.H., C.B.M., C.B., J.B., A.M., R.H., B.B.; supervision, M.H., C.B.M., C.B., J.B., A.M., R.H., B.B.; funding acquisition, C.B., J.B., A.M., R.H., B.B. All authors have read and agreed to the published version of the manuscript.

Institutional Review Board Statement: Not applicable.

Informed Consent Statement: Not applicable.

References

1. Rocha, L.S.; Pereira, D.; Sousa, É.; Otero, M.; Esteves, V.I.; Calisto, V. Recent advances on the development and application of magnetic activated carbon and char for the removal of pharmaceutical compounds from waters: A review. *Sci. Total Environ.* **2020**, *718*, 137272. [CrossRef]
2. Nikolaou, A.; Meric, S.; Fatta, D. Occurrence patterns of pharmaceuticals in water and wastewater environments. *Anal. Bioanal. Chem.* **2007**, *387*, 1225–1234. [CrossRef]
3. Couto, C.F.; Lange, L.C.; Amaral, M.C.S. Occurrence, fate and removal of pharmaceutically active compounds (PhACs) in water and wastewater treatment plants—A review. *J. Water Process Eng.* **2019**, *32*, 100927. [CrossRef]
4. Fonseca Couto, C.; Lange, L.C.; Santos Amaral, M.C. A critical review on membrane separation processes applied to remove pharmaceutically active compounds from water and wastewater. *J. Water Process Eng.* **2018**, *26*, 156–175. [CrossRef]
5. Madikizela, L.M.; Ncube, S.; Chimuka, L. Analysis, occurrence and removal of pharmaceuticals in African water resources: A current status. *J. Environ. Manag.* **2020**, *253*, 109741. [CrossRef] [PubMed]
6. Kümmerer, K. Resistance in the environment. *J. Antimicrob. Chemother.* **2004**, *54*, 311–320. [CrossRef] [PubMed]
7. Żur, J.; Wojcieszyńska, D.; Hupert-Kocurek, K.; Marchlewicz, A.; Guzik, U. Paracetamol—Toxicity and microbial utilization. Pseudomonas moorei KB4 as a case study for exploring degradation pathway. *Chemosphere* **2018**, *206*, 192–202. [CrossRef]
8. Audino, F.; Santamaria, J.M.T.; Del Valle Mendoza, L.J.; Graells, M.; Pérez-Moya, M. Removal of paracetamol using effective advanced oxidation processes. *Int. J. Environ. Res. Public Health* **2019**, *16*, 505. [CrossRef]
9. Li, Y.; Niu, J.; Yin, L.; Wang, W.; Bao, Y.; Chen, J.; Duan, Y. Photocatalytic degradation kinetics and mechanism of pentachlorophenol based on Superoxide radicals. *J. Environ. Sci.* **2011**, *23*, 1911–1918. [CrossRef]
10. Quesada-Penate, I.; Julcour-Lebigue, C.; Jauregui-Haza, U.J.; Wilhelm, A.-M.; Delmas, H. Degradation of paracetamol by catalytic wet air oxidation and sequential adsorption—Catalytic wet air oxidation on activated carbons. *J. Hazard. Mater.* **2012**, *221–222*. [CrossRef]
11. Peñas-Garzón, M.; Gómez-Avilés, A.; Belver, C.; Rodriguez, J.J.; Bedia, J. Degradation pathways of emerging contaminants using TiO_2-activated carbon heterostructures in aqueous solution under simulated solar light. *Chem. Eng. J.* **2020**, *392*, 124867. [CrossRef]
12. Gómez-Avilés, A.; Peñas-Garzón, M.; Bedia, J.; Dionysiou, D.D.; Rodríguez, J.J.; Belver, C. Mixed Ti-Zr metal-organic-frameworks for the photodegradation of acetaminophen under solar irradiation. *Appl. Catal. B Environ.* **2019**, *253*, 253–262. [CrossRef]
13. Rueda Márquez, J.; Levchuk, I.; Sillanpää, M. Application of Catalytic Wet Peroxide Oxidation for Industrial and Urban Wastewater Treatment: A Review. *Catalysts* **2018**, *8*, 673. [CrossRef]
14. Arredondo Valdez, H.C.; García Jiménez, G.; Gutiérrez Granados, S.; Ponce de León, C. Degradation of paracetamol by advance oxidation processes using modified reticulated vitreous carbon electrodes with TiO_2 and $CuO/TiO_2/Al_2O_3$. *Chemosphere* **2012**, *89*, 1195–1201. [CrossRef]
15. Hernández, R.; Olvera-Rodríguez, I.; Guzmán, C.; Medel, A.; Escobar-Alarcón, L.; Brillas, E.; Sirés, I.; Esquivel, K. Microwave-assisted sol-gel synthesis of an Au-TiO_2 photoanode for the advanced oxidation of paracetamol as model pharmaceutical pollutant. *Electrochem. Commun.* **2018**, *96*, 42–46. [CrossRef]
16. Yun, W.C.; Lin, K.Y.A.; Tong, W.C.; Lin, Y.F.; Du, Y. Enhanced degradation of paracetamol in water using sulfate radical-based advanced oxidation processes catalyzed by 3-dimensional Co_3O_4 nanoflower. *Chem. Eng. J.* **2019**, *373*, 1329–1337. [CrossRef]
17. Pires, J.; Borges, S.; Carvalho, A.; Pereira, C.; Pereira, A.M.; Fernandes, C.; Araújo, J.P.; Freire, C. Magnetically recyclable mesoporous iron oxide-silica materials for the degradation of acetaminophen in water under mild conditions. *Polyhedron* **2016**, *106*, 125–131. [CrossRef]
18. Mao, H.; Ji, C.; Liu, M.; Cao, Z.; Sun, D.; Xing, Z.; Chen, X.; Zhang, Y.; Song, X.M. Enhanced catalytic activity of Ag nanoparticles supported on polyacrylamide/polypyrrole/graphene oxide nanosheets for the reduction of 4-nitrophenol. *Appl. Surf. Sci.* **2018**, *434*, 522–533. [CrossRef]
19. Adityosulindro, S.; Julcour, C.; Barthe, L. Heterogeneous Fenton oxidation using Fe-ZSM5 catalyst for removal of ibuprofen in wastewater. *J. Environ. Chem. Eng.* **2018**, *6*, 5920–5928. [CrossRef]
20. Carrasco-Díaz, M.R.; Castillejos-López, E.; Cerpa-Naranjo, A.; Rojas-Cervantes, M.L. On the textural and crystalline properties of Fe-carbon xerogels. Application as Fenton-like catalysts in the oxidation of paracetamol by H_2O_2. *Microporous Mesoporous Mater.* **2017**, *237*, 282–293. [CrossRef]
21. Hurtado, L.; Romero, R.; Mendoza, A.; Brewer, S.; Donkor, K.; Gómez-Espinosa, R.M.; Natividad, R. Paracetamol mineralization by Photo Fenton process catalyzed by a Cu/Fe-PILC under circumneutral pH conditions. *J. Photochem. Photobiol. A Chem.* **2019**, *373*, 162–170. [CrossRef]
22. Peng, A.; Huang, M.; Chen, Z.; Gu, C. Oxidative coupling of acetaminophen mediated by Fe3 +-saturated montmorillonite. *Sci. Total Environ.* **2017**, *595*, 673–680. [CrossRef] [PubMed]
23. Crowther, N.; Larachi, F. Iron-containing silicalites for phenol catalytic wet peroxidation. *Appl. Catal. B Environ.* **2003**, *46*, 293–305. [CrossRef]

24. Gokulakrishnan, N.; Pandurangan, A.; Sinha, P.K. Catalytic wet peroxide oxidation technique for the removal of decontaminating agents ethylenediaminetetraacetic acid and oxalic acid from aqueous solution using efficient fenton type Fe-MCM-41 mesoporous materials. *Ind. Eng. Chem. Res.* **2009**, *48*, 1556–1561. [CrossRef]

25. Yan, Y.; Wu, X.; Zhang, H. Catalytic wet peroxide oxidation of phenol over Fe_2O_3/MCM-41 in a fixed bed reactor. *Sep. Purif. Technol.* **2016**, *171*, 52–61. [CrossRef]

26. Hakiki, A.; Boukoussa, B.; Habib Zahmani, H.; Hamacha, R.; Hadj Abdelkader, N.e.H.; Bekkar, F.; Bettahar, F.; Nunes-Beltrao, A.P.; Hacini, S.; Bengueddach, A.; et al. Synthesis and characterization of mesoporous silica SBA-15 functionalized by mono-, di-, and tri-amine and its catalytic behavior towards Michael addition. *Mater. Chem. Phys.* **2018**, *212*, 415–425. [CrossRef]

27. Boukoussa, B.; Hakiki, A.; Nunes-Beltrao, A.P.; Hamacha, R.; Azzouz, A. Assessment of the intrinsic interactions of nanocomposite polyaniline/SBA-15 with carbon dioxide: Correlation between the hydrophilic character and surface basicity. *J. CO2 Util.* **2018**, *26*, 171–178. [CrossRef]

28. Boukoussa, B.; Hakiki, A.; Moulai, S.; Chikh, K.; Kherroub, D.E.; Bouhadjar, L.; Guedal, D.; Messaoudi, K.; Mokhtar, F.; Hamacha, R. Adsorption behaviors of cationic and anionic dyes from aqueous solution on nanocomposite polypyrrole/SBA-15. *J. Mater. Sci.* **2018**, *53*, 7372–7386. [CrossRef]

29. Boukoussa, B.; Kibou, Z.; Abid, Z.; Ouargli, R.; Choukchou-Braham, N.; Villemin, D.; Bengueddach, A.; Hamacha, R. Key factor affecting the basicity of mesoporous silicas MCM-41: Effect of surfactant extraction time and Si/Al ratio. *Chem. Pap.* **2018**, *72*, 289–299. [CrossRef]

30. Boukoussa, B.; Zeghada, S.; Ababsa, G.B.; Hamacha, R.; Derdour, A.; Bengueddach, A.; Mongin, F. Catalytic behavior of surfactant-containing-MCM-41 mesoporousmaterials for cycloaddition of 4-nitrophenyl azide. *Appl. Catal. A Gen.* **2015**, *489*, 131–139. [CrossRef]

31. Iglesias, J.; Melero, J.A.; Sánchez-Sánchez, M. Highly Ti-loaded MCM-41: Effect of the metal precursor and loading on the titanium distribution and on the catalytic activity in different oxidation processes. *Microporous Mesoporous Mater.* **2010**, *132*, 112–120. [CrossRef]

32. Asghari, S.; Haghighi, M.; Taghavinezhad, P. Plasma-enhanced dispersion of Cr_2O_3 over ceria-doped MCM-41 nanostructured catalyst used in CO_2 oxidative dehydrogenation of ethane to ethylene. *Microporous Mesoporous Mater.* **2019**, *279*, 165–177. [CrossRef]

33. Mohamed, A.S.; AbuKhadra, M.R.; Abdallah, E.A.; El-Sherbeeny, A.M.; Mahmoud, R.K. The photocatalytic performance of silica fume based Co_3O_4/MCM-41 green nanocomposite for instantaneous degradation of Omethoate pesticide under visible light. *J. Photochem. Photobiol. A Chem.* **2020**, *392*, 112434. [CrossRef]

34. Nidheesh, P.V. Heterogeneous Fenton catalysts for the abatement of organic pollutants from aqueous solution: A review. *RSC Adv.* **2015**, *5*, 40552–40577. [CrossRef]

35. Sádaba, I.; López Granados, M.; Riisager, A.; Taarning, E. Deactivation of solid catalysts in liquid media: The case of leaching of active sites in biomass conversion reactions. *Green Chem.* **2015**, *17*, 4133–4145. [CrossRef]

36. Meynen, V.; Cool, P.; Vansant, E.F. Verified syntheses of mesoporous materials. *Microporous Mesoporous Mater.* **2009**, *125*, 170–223. [CrossRef]

37. Kruk, M.; Jaroniec, M.; Kim, J.M.; Ryoo, R. Characterization of highly ordered MCM-41 silicas using X-ray diffraction and nitrogen adsorption. *Langmuir* **1999**, *15*, 5279–5284. [CrossRef]

38. Abrokwah, R.Y.; Deshmane, V.G.; Kuila, D. Comparative performance of M-MCM-41 (M: Cu, Co, Ni, Pd, Zn and Sn) catalysts for steam reforming of methanol. *J. Mol. Catal. A Chem.* **2016**, *425*, 10–20. [CrossRef]

39. Campos, C. New perspectives on microbiological water control for wastewater reuse. *Desalination* **2008**, *218*, 34–42. [CrossRef]

40. Hao, X.; Zhang, Y.; Wang, J.; Zhou, W.; Zhang, C.; Liu, S. A novel approach to prepare MCM-41 supported CuO catalyst with high metal loading and dispersion. *Microporous Mesoporous Mater.* **2006**, *88*, 38–47. [CrossRef]

41. Balasubramanian, C.; Joseph, B.; Gupta, P.; Saini, N.L.; Mukherjee, S.; Di Gioacchino, D.; Marcelli, D. X-ray absorption spectroscopy characterization of iron-oxide nanoparticles synthesized by high temperature plasma processing. *J. Electron Spectrosc. Relat. Phenom.* **2014**, *196*, 125–129. [CrossRef]

42. Ursachi, I.; Stancu, A.; Vasile, A. Magnetic α-Fe_2O_3/MCM-41 nanocomposites: Preparation, characterization, and catalytic activity for methylene blue degradation. *J. Colloid Interface Sci.* **2012**, *377*, 184–190. [CrossRef]

43. Numan, M.; Kim, T.; Jo, C.; Park, S.-E. Ethane Dehydrogenation with CO_2 as a soft oxidant over a Cr-TUD-1 catalyst. *J. CO2 Util.* **2020**, *39*, 101184. [CrossRef]

44. Al-Awadi, A.S.; El-Toni, A.M.; Al-Zahrani, S.M.; Abasaeed, A.E.; Khan, A. Synthesis, Characterization and Catalytic Evaluation of Chromium Oxide Deposited on Titania–Silica Mesoporous Nanocomposite for the Ethane Dehydrogenation with CO_2. *Crystals* **2020**, *10*, 322. [CrossRef]

45. Mahendiran, C.; Sangeetha, P.; Vijayan, P.; Sardhar Basha, S.J.; Shanthi, K. Vapour phase oxidation of tetralin over Cr and Fe substituted MCM-41 molecular sieves. *J. Mol. Catal. A Chem.* **2007**, *275*, 84–90. [CrossRef]

46. Hao, T.; Yang, C.; Rao, X.; Wang, J.; Niu, C.; Su, X. Facile additive-free synthesis of iron oxide nanoparticles for efficient adsorptive removal of Congo red and Cr(VI). *Appl. Surf. Sci.* **2014**, *292*, 174–180. [CrossRef]

47. Cuesta Zapata, P.M.; Gonzo, E.E.; Parentis, M.L.; Bonini, N.A. Acidity evolution on highly dispersed chromium supported on mesostructured silica: The effect of hydrothermal treatment and calcination temperature. *Microporous Mesoporous Mater.* **2020**, *294*, 109895. [CrossRef]

48. Sharma, S.K.; Sudarshan, K.; Sen, D.; Pujari, P.K. Microenvironment of mesopores of MCM-41 supported CuO catalyst: An investigation using positronium probe. *J. Solid State Chem.* **2019**, *274*, 10–17. [CrossRef]

49. Kowalczyk, A.; Borcuch, A.; Michalik, M.; Rutkowska, M.; Gil, B.; Sojka, Z.; Indyka, P.; Chmielarz, L. MCM-41 modified with transition metals by template ion-exchange method as catalysts for selective catalytic oxidation of ammonia to dinitrogen. *Microporous Mesoporous Mater.* **2017**, *240*, 9–21. [CrossRef]

50. Machado, P.M.A.; Lube, L.M.; Tiradentes, M.D.E.; Fernandes, C.; Gomes, C.A.; Stumbo, A.M.; San Gil, R.A.S.; Visentin, L.C.; Sanchez, D.R.; Frescura, V.L.A.; et al. Synthesis, characterization and activity of homogeneous and heterogeneous (SiO₂, NaY, MCM-41) iron(III) catalysts on cyclohexane and cyclohexene oxidation. *Appl. Catal. A Gen.* **2015**, *507*, 119–129. [CrossRef]

51. Sekkiou, H.; Boukoussa, B.; Ghezini, R.; Khenchoul, Z.; Ouali, A.; Hamacha, R.; Bengueddach, A. Enhanced hydrogen storage capacity of copper containing mesoporous silicas prepared using different methods. *Mater. Res. Express* **2016**, *3*, 085501. [CrossRef]

52. Huo, C.; Ouyang, J.; Yang, H. CuO nanoparticles encapsulated inside Al-MCM-41 mesoporous materials via direct synthetic route. *Sci. Rep.* **2015**, *4*, 1–9. [CrossRef] [PubMed]

53. Wang, L.; Sang, S.; Meng, S.; Zhang, Y.; Qi, Y.; Liu, Z. Direct synthesis of Zn-ZSM-5 with novel morphology. *Mater. Lett.* **2007**, *61*, 1675–1678. [CrossRef]

54. Alarcón, E.A.; Villa, A.L.; de Correa, C.M. Characterization of Sn- and Zn-loaded MCM-41 catalysts for nopol synthesis. *Microporous Mesoporous Mater.* **2009**, *122*, 208–215. [CrossRef]

55. Hur, S.G.; Kim, T.W.; Hwang, S.J.; Hwang, S.H.; Yang, J.H.; Choy, J.H. Heterostructured nanohybrid of zinc oxide-montmorillonite clay. *J. Phys. Chem. B* **2006**, *110*, 1599–1604. [CrossRef] [PubMed]

56. Al-Awadi, A.S.; El-Toni, A.M.; Alhoshan, M.; Khan, A.; Labis, J.P.; Al-Fatesh, A.; Abasaeed, A.E.; Al-Zahrani, S.M. Impact of precursor sequence of addition for one-pot synthesis of Cr-MCM-41 catalyst nanoparticles to enhance ethane oxidative dehydrogenation with carbon dioxide. *Ceram. Int.* **2019**, *45*, 1125–1134. [CrossRef]

57. Savidha, R.; Pandurangan, A.; Palanichamy, M.; Murugesan, V. A comparative study on the catalytic activity of Zn and Fe containing Al-MCM-41 molecular sieves on t-butylation of phenol. *J. Mol. Catal. A Chem.* **2004**, *211*, 165–177. [CrossRef]

58. Wang, Y.; Zhang, Q.; Shishido, T.; Takehira, K. Characterizations of Iron-Containing MCM-41 and Its Catalytic Properties in Epoxidation of Styrene with Hydrogen Peroxide. *J. Catal.* **2002**, *209*, 186–196. [CrossRef]

59. Balouria, V.; Kumar, A.; Singh, A.; Samanta, S.; Debnath, A.K.; Mahajan, A.; Bedi, R.K.; Aswal, D.K.; Gupta, S.K.; Yakhmi, J.V. Temperature dependent H₂S and Cl2 sensing selectivity of Cr₂O₃ thin films. *Sens. Actuators B Chem.* **2011**, *157*, 466–472. [CrossRef]

60. Wright, K.; Barron, A. Catalyst Residue and Oxygen Species Inhibition of the Formation of Hexahapto-Metal Complexes of Group 6 Metals on Single-Walled Carbon Nanotubes. *J. Carbon Res.* **2017**, *3*, 17. [CrossRef]

61. Wang, X.; Liu, Q.; Xiao, Z.; Chen, X.; Shi, C.; Tao, S.; Huang, Y.; Liang, C. In situ synthesis of Au-Pd bimetallic nanoparticles on amine-functionalized SiO₂ for the aqueous-phase hydrodechlorination of chlorobenzene. *RSC Adv.* **2014**, *4*, 48254–48259. [CrossRef]

62. Chen, L.F.; Guo, P.J.; Qiao, M.H.; Yan, S.R.; Li, H.X.; Shen, W.; Xu, H.L.; Fan, K.N. Cu/SiO₂ catalysts prepared by the ammonia-evaporation method: Texture, structure, and catalytic performance in hydrogenation of dimethyl oxalate to ethylene glycol. *J. Catal.* **2008**, *257*, 172–180. [CrossRef]

63. Zheng, J.; Chen, Z.; Fang, J.; Wang, Z.; Zuo, S. MCM-41 supported nano-sized CuO-CeO₂ for catalytic combustion of chlorobenzene. *J. Rare Earths* **2020**. [CrossRef]

64. Bozzini, B.; Griskonis, E.; Fanigliulo, A.; Sulcius, A. Electrodeposition of Zn-Mn alloys in the presence of thiocarbamide. *Surf. Coat. Technol.* **2002**, *154*, 294–303. [CrossRef]

65. Yang, L.L.; Zhao, Q.X.; Willander, M.; Liu, X.J.; Fahlman, M.; Yang, J.H. Origin of the surface recombination centers in ZnO nanorods arrays by X-ray photoelectron spectroscopy. *Appl. Surf. Sci.* **2010**, *256*, 3592–3597. [CrossRef]

66. Sett, D.; Basak, D. Tuning the luminescence and UV photosensing properties of ZnO nanorods by strategic aqueous chemical growth. *Mater. Res. Express* **2015**, *2*, 105008. [CrossRef]

67. Jin, M.; Yang, R.; Zhao, M.; Li, G.; Hu, C. Application of Fe/activated carbon catalysts in the hydroxylation of phenol to dihydroxybenzenes. *Ind. Eng. Chem. Res.* **2014**, *53*, 2932–2939. [CrossRef]

68. Yamashita, T.; Hayes, P. Analysis of XPS spectra of Fe 2+ and Fe 3+ ions in oxide materials. *Appl. Surf. Sci.* **2008**, *254*, 2441–2449. [CrossRef]

69. Nie, Y.; Li, N.; Hu, C. Enhanced inhibition of bromate formation in catalytic ozonation of organic pollutants over Fe-Al LDH/Al₂O₃. *Sep. Purif. Technol.* **2015**, *151*, 256–261. [CrossRef]

70. Cuello, N.I.; Elías, V.R.; Rodriguez Torres, C.E.; Crivello, M.E.; Oliva, M.I.; Eimer, G.A. Development of iron modified MCM-41 as promising nano-composites with specific magnetic behavior. *Microporous Mesoporous Mater.* **2015**, *203*, 106–115. [CrossRef]

71. Decolatti, H.P.; Gioria, E.G.; Ibarlín, S.N.; Navascués, N.; Irusta, S.; Miró, E.E.; Gutierrez, L.B. Exchanged lanthanum in InHMOR and its impact on the catalytic performance of InHMOR. Spectroscopic, volumetric and microscopic studies. *Microporous Mesoporous Mater.* **2016**, *222*, 9–22. [CrossRef]

72. Zhang, J.; Wong, H.; Kakushima, K.; Iwai, H. XPS study on the effects of thermal annealing on CeO₂/La₂O₃ stacked gate dielectrics. *Thin Solid Films* **2016**, *600*, 30–35. [CrossRef]

73. Zheng, Z.; Wang, J.; Wei, Y.; Liu, X.; Yu, F.; Ji, J. Effect of La-Fe/Si-MCM-41 catalysts and CaO additive on catalytic cracking of soybean oil for biofuel with low aromatics. *J. Anal. Appl. Pyrolysis* **2019**, *143*, 104693. [CrossRef]

74. Akpotu, S.O.; Moodley, B. Application of as-synthesised MCM-41 and MCM-41 wrapped with reduced graphene oxide/graphene oxide in the remediation of acetaminophen and aspirin from aqueous system. *J. Environ. Manag.* **2018**, *209*, 205–215. [CrossRef]

75. Kong, S.H.; Watts, R.J.; Choi, J.H. Treatment of petroleum-contaminated soils using iron mineral catalyzed hydrogen peroxide. *Chemosphere* **1998**, *37*, 1473–1482. [CrossRef]

76. Huang, H.H.; Lu, M.C.; Chen, J.N. Catalytic decomposition of hydrogen peroxide and 2-chlorophenol with iron oxides. *Water Res.* **2001**, *35*, 2291–2299. [CrossRef]

77. Pliego, G.; Zazo, J.A.; Garcia-Muñoz, P.; Munoz, M.; Casas, J.A.; Rodriguez, J.J. Trends in the Intensification of the Fenton Process for Wastewater Treatment: An Overview. *Crit. Rev. Environ. Sci. Technol.* **2015**, *45*, 2611–2692. [CrossRef]

78. Pereira, M.C.; Oliveira, L.C.A.; Murad, E. Iron oxide catalysts: Fenton and Fentonlike reactions—A review. *Clay Miner.* **2012**, *47*, 285–302. [CrossRef]

79. Bokare, A.D.; Choi, W. Review of iron-free Fenton-like systems for activating H_2O_2 in advanced oxidation processes. *J. Hazard. Mater.* **2014**, *275*, 121–135. [CrossRef]

80. Zazo, J.A.; Casas, J.A.; Molina, C.B.; Quintanilla, A.; Rodriguez, J.J. Evolution of ecotoxicity upon Fenton's oxidation of phenol in water. *Environ. Sci. Technol.* **2007**, *41*, 7164–7170. [CrossRef] [PubMed]

81. Olvera-Vargas, H.; Rouch, J.C.; Coetsier, C.; Cretin, M.; Causserand, C. Dynamic cross-flow electro-Fenton process coupled to anodic oxidation for wastewater treatment: Application to the degradation of acetaminophen. *Sep. Purif. Technol.* **2018**, *203*, 143–151. [CrossRef]

82. Le, T.X.H.; Van Nguyen, T.; Amadou Yacouba, Z.; Zoungrana, L.; Avril, F.; Nguyen, D.L.; Petit, E.; Mendret, J.; Bonniol, V.; Bechelany, M.; et al. Correlation between degradation pathway and toxicity of acetaminophen and its by-products by using the electro-Fenton process in aqueous media. *Chemosphere* **2017**, *172*, 1–9. [CrossRef] [PubMed]

83. Orimolade, B.O.; Zwane, B.N.; Koiki, B.A.; Rivallin, M.; Bechelany, M.; Mabuba, N.; Lesage, G.; Cretin, M.; Arotiba, O.A. Coupling cathodic electro-fenton with anodic photo-electrochemical oxidation: A feasibility study on the mineralization of paracetamol. *J. Environ. Chem. Eng.* **2020**, *8*, 104394. [CrossRef]

84. Boukoussa, B.; Hamacha, R.; Morsli, A.; Bengueddach, A. Adsorption of yellow dye on calcined or uncalcined Al-MCM-41 mesoporous materials. *Arab. J. Chem.* **2017**, *10*, S2160–S2169. [CrossRef]

85. Brezoiu, A.M.; Deaconu, M.; Nicu, I.; Vasile, E.; Mitran, R.A.; Matei, C.; Berger, D. Heteroatom modified MCM-41-silica carriers for Lomefloxacin delivery systems. *Microporous Mesoporous Mater.* **2019**, *275*, 214–222. [CrossRef]

86. Eisenberg, G.M. Colorimetric Determination of Hydrogen Peroxide. *Ind. Eng. Chem. Anal. Ed.* **1943**, *15*, 327–328. [CrossRef]